ACS NANO

www.acsnano.org

ARTICLE

Improving Lithium Metal Composite Anodes with Seeding and Pillaring Effects of Silicon Nanoparticles

Hansen Wang, Xia Cao, Hanke Gu, Yayuan Liu, Yanbin Li, Zewen Zhang, William Huang, Hongxia Wang, Jiangyan Wang, Wu Xu, Ji-Guang Zhang, and Yi Cui*

Cite This: *ACS Nano* 2020, 14, 4601−4608

Read Online

ACCESS | Metrics & More | Article Recommendations | Supporting Information

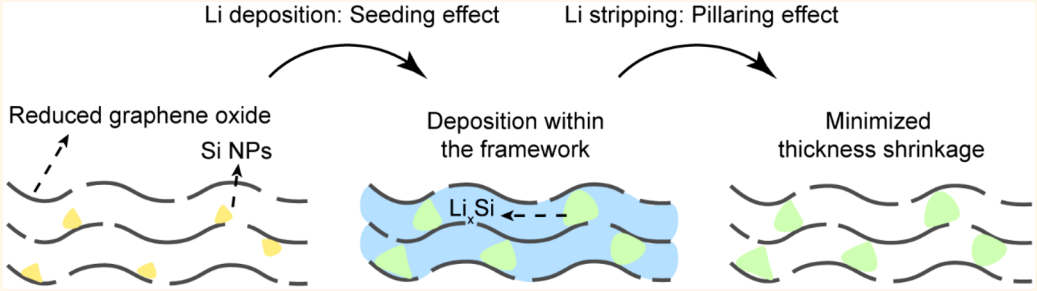

ABSTRACT: **Metallic lithium (Li) anodes are crucial for the development of high specific energy batteries yet are plagued by their poor cycling efficiency. Electrode architecture engineering is vital for maintaining a stable anode volume and suppressing Li corrosion during cycling. In this paper, a reduced graphene oxide "host" framework for Li metal anodes is further optimized by embedding silicon (Si) nanoparticles between the graphene layers. They serve as Li nucleation seeds to promote Li deposition within the framework even without prestored Li. Meanwhile, the Li$_x$Si alloy particles serve as supporting "pillars" between the graphene layers, enabling a minimized thickness shrinkage after full stripping of metallic Li. Combined with a Li compatible electrolyte, a 99.4% Coulombic efficiency over ∼600 cycles is achieved, and stable cycling of a Li||NMC532 full cell for ∼380 cycles with negligible capacity decay is realized.**

KEYWORDS: *Li metal anode, host, graphene oxide, Si nanoparticles, nucleation seeds, pillaring effect*

Metallic lithium (Li) is the ultimate choice of anode material for next-generation high specific energy batteries due to its low electrode potential and high specific capacity.[1] Nevertheless, its dendritic growth, uncontrollable large volume change during cycling, and subsequent low Coulombic efficiency (CE) in conventional Li-ion battery electrolytes undermine its operational safety and cycle life.[2−5] Great efforts were made to address the key issues of metallic Li anodes. Among them, two methodologies are widely acknowledged to be effective for the improvement of the cycling performance of metallic Li anodes.

Maintaining a stable anode volume during cycling is critical.[1,3,6] The significant volume change of metallic Li roots from its "host-free" nature. The volume change causes the solid electrolyte interphase (SEI) to easily crack, exposing fresh Li surface. This leads to further SEI formation, dendritic growth, and aggravated Li inventory losses. The "host" concept aimed at suppressing volume fluctuation was first proposed in two exciting examples of seeded hollow carbon spheres[7] and layered graphene oxides (GO),[8] followed by a series of other demonstrations of artificial "host" frameworks.[7−17] They successfully promoted the cycle life of metallic Li anodes, yet still demanded further improvements. For example, Li-reduced graphene oxide (rGO) composite anode still showed a ∼20% of volume change after full stripping of metallic Li.[8] Besides, a certain amount of metallic Li needed to be maintained within the framework as the "seed" for Li deposition. Otherwise, Li would preferentially deposit on the outer surface due to the

Received: January 8, 2020
Accepted: April 9, 2020
Published: April 9, 2020

https://dx.doi.org/10.1021/acsnano.0c00184
ACS Nano 2020, 14, 4601−4608

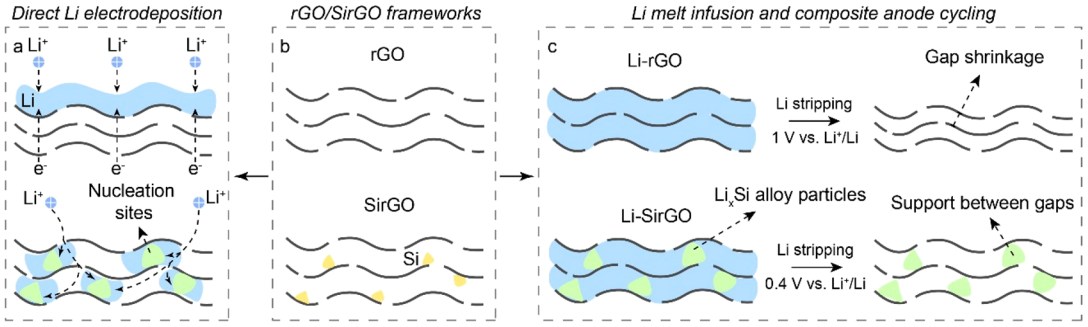

Figure 1. Schematic drawings showing the advantages of SirGO over conventional rGO framework. (a) After direct deposition, metallic Li plates on the top surface of rGO, while preferentially deposits into the SirGO framework due to the seeding effect of Si nanoparticles. (b) Schematic of rGO and SirGO frameworks. (c) After Li melt infusion and stripping, the thickness of Li-rGO composite anode shrinks, while that of the Li-SirGO composite anode maintains due to the pillaring effect of the Li_xSi particles remaining within the gaps.

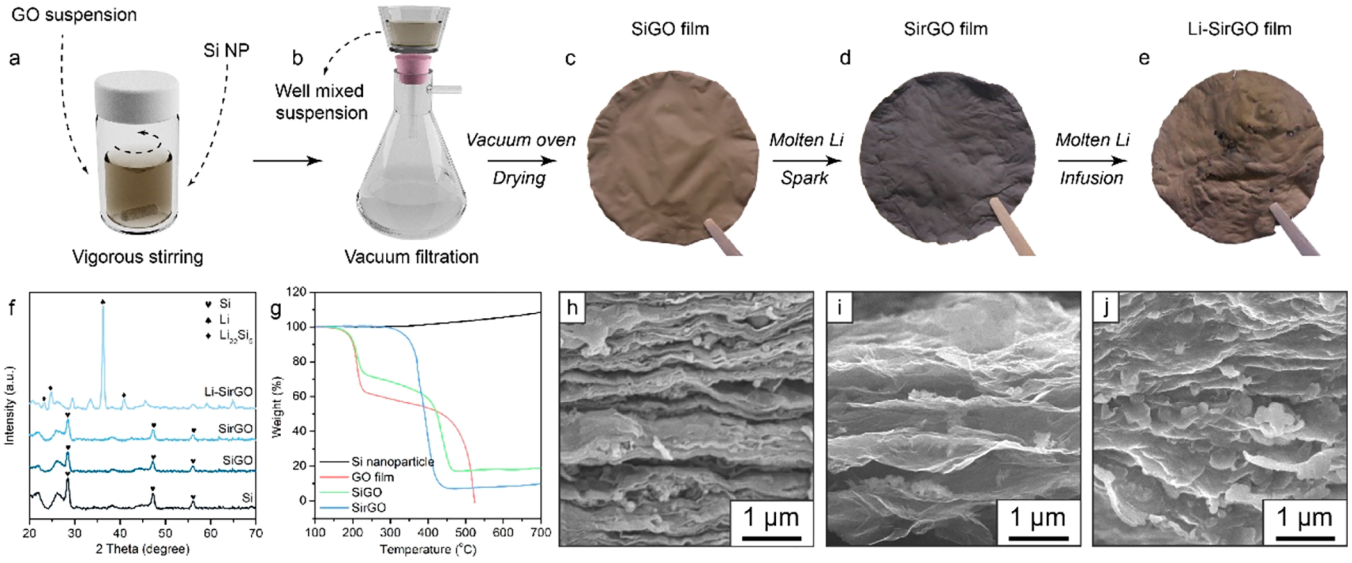

Figure 2. Fabrication and characterization of Li-SirGO. (a–e) Fabrication procedure of Li-SirGO composite anode. GO aqueous suspension is first mixed with Si nanoparticles under vigorous stirring (a). Then the suspension is vacuum filtered (b) and dried to form SiGO film (c). The SiGO film goes through spark reaction with molten Li to form SirGO film (d). Finally, metallic Li is infused into the framework to form Li-SirGO composite anode (e). (f) XRD patterns of Si nanoparticle, SiGO, SirGO and Li-SirGO films. (g) TGA results of Si nanoparticle, GO, SiGO, and SirGO films in simulated air atmosphere (20% O_2 + 80% Ar). (h–j) SEM images of the cross sections of SiGO film (h), SirGO film (i), and Li-SirGO film (j).

electronic conductivity of the rGO framework and the corresponding protection would be lost.

To build a stable SEI to passivate the highly reactive Li metal, electrolyte engineering is a crucial approach.[3,18] Commercial $LiPF_6$/carbonate electrolytes are optimized for Li-ion batteries, but are not ideal for the cycling of metallic Li anodes. Recently, ether-based, highly fluorinated chemicals were widely developed as solvents in electrolytes for metallic Li anodes.[19−22] With the idea of localized high-concentration electrolytes (LHCEs),[23−27] the cycling performance of metallic Li was improved to a higher level. Although the metallic Li deposits showed a much more homogeneous morphology within these electrolytes, they were still far from perfectly dense films. Meanwhile, the volume and pressure fluctuation remained during cycling, undermining long-term stable cycling capability. Therefore, a synergetic method combining well optimized "host" structures with high-performance electrolytes is urgently demanded.[3]

In this work, a framework of silicon (Si) nanoparticles embedded reduced graphene oxide (SirGO) is fabricated as a further improved "host" for metallic Li. The Si nanoparticles afford two critical effects compared to previous Li metal "host" frameworks. First, they serve as nucleation seeds for metallic Li deposition. This suppresses Li deposition outside the framework and facilitates better protection of Li deposited into the "host" (Figure 1a). Second, the subsequently formed Li_xSi alloy particles serve as structure supporting "pillars" to maintain the gap spaces between graphene layers, leading to a minimized thickness shrinkage even after full stripping of metallic Li (Figure 1c). With a recently reported high-performance LHCE based on tris(2,2,2-trifluoroethyl)-orthoformate (TFEO)[28] to build a monolithic SEI, the SirGO host shows excellent electrochemical performances. Li||SirGO half cells provide stable a CE of 99.4% for over 600 cycles. Furthermore, Li-SirGO||NMC532 full cells (N/P ratio ≈4) can be cycled for ∼380 cycles with negligible capacity decay. This work optimizes Li metal host structures with the seeding and pillaring effects of Si nanoparticles and achieves excellent full cell performance by incorporating a state-of-the-

https://dx.doi.org/10.1021/acsnano.0c00184
ACS Nano 2020, 14, 4601−4608

art electrolyte, representing a significant advancement for the Li metal battery development.

RESULTS AND DISCUSSION

Figure 2a–e shows the synthesis procedure of Li-SirGO composite anodes. Si nanoparticles with ~100 nm diameters (Figure S1) are first uniformly dispersed in GO solutions through vigorous stirring and sonicating (Figure 2a). The suspension is then vacuum filtered (Figure 2b) to form Si embedded GO (SiGO) films (Figure 2c). Subsequently, SiGO films go through spark reaction to form Si embedded rGO (SirGO) films[8] (Figure 2d) and melt infusion of metallic Li to achieve Li-SirGO composite anodes (Figure 2e). Figure 2h–j is scanning electron microscopy (SEM) images of the cross sections for SiGO, SirGO, and Li-SirGO films. The gaps between graphene layers expand significantly after the spark reaction, and the embedded Si nanoparticles can be observed (Figure 2i). After Li infusion, the gaps are filled with metallic Li, and particles resembling the morphology of Li_xSi alloy appear (Figure 2j). Energy dispersive X-ray spectroscopy (EDS) is performed on the cross sections of SirGO and Li-SirGO films (Figure S2), confirming the uniform distribution of Si between the graphene layers. Top-views of the films are shown in Figure S3. X-ray diffraction (XRD) patterns (Figure 2f) confirm the formation of Li_xSi alloy with the highest Li ratio ($Li_{22}Si_5$), which is made possible by the high temperature (400 °C) provided during the melt infusion process. Thermogravimetric analysis (TGA) is performed under simulated air atmosphere (20% oxygen (O_2) + 80% argon (Ar)) to characterize the mass ratio of Si within the "host" framework (Figure 2g). GO and SiGO samples show an extra mass loss plateau at ~200 °C compared to SirGO, which can be attributed to the decomposition of oxygen-containing functional groups and the release of H_2O, CO and CO_2 molecules.[29] Calculated from the curve of the SirGO sample, Si nanoparticles occupy ~7% of the mass of the SirGO framework. The Li-SirGO composite anode offers a high specific capacity of 3089 mAh/g (Figure S4). A second voltage plateau at ~0.4 V can be observed, corresponding to the decomposition of Li_xSi. These Li_xSi particles contribute to only ~5% of the total capacity, so the specific capacity of the composite anode is not undermined, while only the metallic Li is utilized during cycling.

Si nanoparticles serve as nucleation seeds for metallic Li deposition. Figure 1a schematically illustrates this effect. When Li is directly deposited onto an rGO film, the high electronic conductivity of the rGO framework causes metallic Li to preferentially plate on the top surface. In this case, the metallic Li directly contacts with the electrolyte and loses the protection from the framework. Consequently, the conventional rGO framework demands prestored Li to function as an effective "host" so that Li would deposit on existing Li instead of forming new nuclei which requires extra overpotential. In contrast, with the existence of Si nanoparticles between the graphene layers, Li first alloys with the Si above 0 V *vs* Li/Li^+ and subsequently precipitates as metallic Li. In this way, Li is fully protected within the SirGO framework even when directly deposited to the "host" without prestored Li, leading to a better rechargeability. A simple experiment is designed to demonstrate this effect. SirGO and rGO films are paired with Li foil in coin cells. Afterward, 1 mAh/cm^2 of Li is deposited onto the SirGO and rGO electrodes, respectively. After coin cell disassembly, a significant amount of silver-colored metallic Li can be observed on top of the rGO film (Figure 3a), while the surface of the SirGO film remains black (Figure 3b). SEM

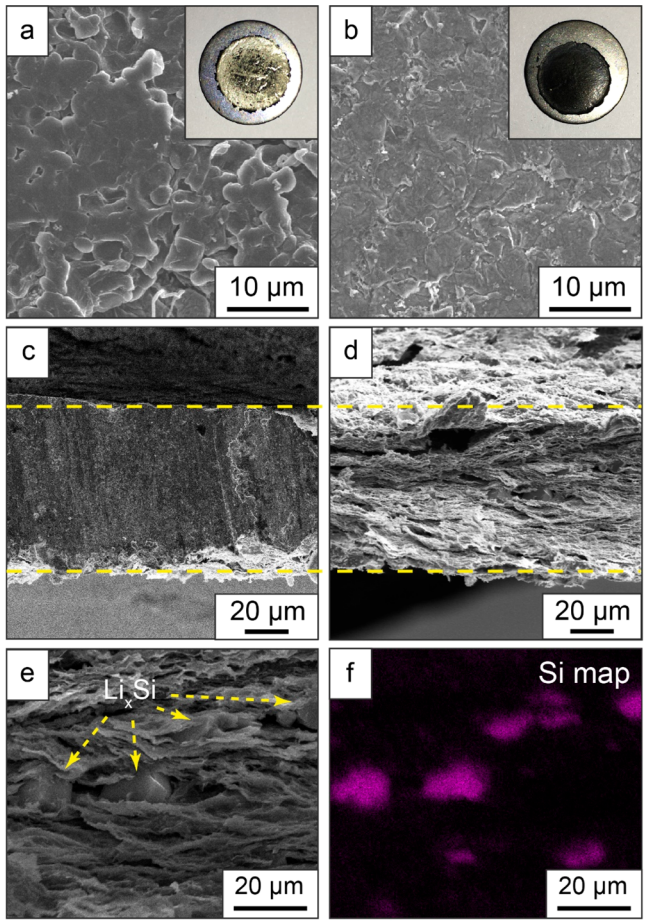

Figure 3. Working mechanisms of SirGO frameworks. (a, b) SEM images and digital photos (inset) of a rGO film (a) and a SirGO film (b) after depositing 1 mAh/cm^2 of Li at 1 mA/cm^2. A significant amount of metallic Li is observed on the top surface of the rGO film, while no metallic Li appears on the top surface of the SirGO film. (c, d) SEM images of the cross sections of a Li-SirGO composite film before (c) and after (d) stripping metallic Li to 0.4 V *vs* Li/Li^+. The sample in (c) is prepared through direct cutting for a sharp edge. (e) SEM image of an enlarged region in (d). Large particles can be observed between the graphene layers. (f) SEM-EDS mapping of Si for the region shown in (e). The particles in (e) are very rich in Si, confirming that they are Li_xSi serving as pillars after Li stripping for a minimized thickness shrinkage.

images also confirm the growth of dendrites on rGO film and a smooth surface without metallic Li of the SirGO film.

Another crucial functionality of the Si nanoparticles is to eliminate the thickness fluctuations during cycling. Li-rGO composite anode still experienced thickness shrinkage after Li stripping.[8] This is caused by the lack of support between the graphene flakes after losing the metallic Li (Figure 1c). It is known that Si has an over 400% volume expansion after full lithiation. Although the embedded Si nanoparticles have diameters of ~100 nm, their dimensions after alloying with Li match that of the gaps between the graphene layers. If we set the cutoff voltage to 0.4 V during the stripping process, all the metallic Li is stripped away, while the Li_xSi particles are maintained. In this way, the distance between the graphene layers is well supported, and a stable anode volume can be

https://dx.doi.org/10.1021/acsnano.0c00184
ACS Nano 2020, 14, 4601–4608

achieved (Figure 1c). To confirm this effect, metallic Li is stripped from a Li-SirGO composite film until 0.4 V *vs* Li/Li$^+$, and the cross sections can be observed in Figure 3c,d. Thickness is also measured at multiple other regions of this film (Figure S5), and statistical analysis results are shown in Table 1. This 69.3 ± 7.00 μm-thick Li-SirGO film shows a

Table 1. Thickness of a Li-SirGO Film before and after Metallic Li Stripping

	thickness (μm)						
	#1	#2	#3	#4	#5	avg.	std.
Li-SirGO	74.3	73.5	63.3	60.2	75.2	69.3	7.00
Li-SirGO (no Li)	72.6	63.7	66.8	65.1	72.6	68.2	4.20

thickness of 68.2 ± 4.20 μm after complete metallic Li stripping. This is only ~1.6% of thickness shrinkage and a significant improvement compared to Li-rGO composite anode.[8] Figure 3e shows an enlarged region in Figure 3d. Large particles can be observed between the graphene layers. SEM-EDS is further performed to confirm the elemental distribution. Si (Figure 3f) and carbon (C) (Figure S6b) maps distinctively show that the particles in Figure 3e are rich in Si and poor in C. An overlay image (Figure S6a) further confirms that the Si distribution matches the particle distribution very well. Considering that the particles sizes are much larger than pristine Si nanoparticles we use, we believe that they are exactly the agglomerated Li$_x$Si alloy particles that we expect to serve as pillars for the graphene layers after metallic Li stripping. This further minimized volume fluctuation will possibly enable an improved long-term stable cycling of the composite anodes.

CE measurements in Li||Cu (copper), Li||rGO, and Li||SirGO half cells (1 mA/cm^2, 1 mAh/cm^2) are first performed to demonstrate the effects of the Si nanoparticles on electrochemical performances (Figure 4a,b and Table 2).

Table 2. Half-Cell CE Analysis

	11−100 cycles		101−600 cycles	
	avg. CE (%)	std. CE (%)	avg. CE (%)	std. CE (%)
Cu foil	98.09	0.549	98.30	3.629
rGO	97.98	0.507	99.54	2.290
SirGO (1.5 V)	99.09	0.934	100.25	5.472
SirGO (0.4 V)	98.40	0.833	99.40	0.247

The electrolyte used here is 1 M LiFSI/DME-TFEO. Due to its high compatibility to metallic Li, bare Cu foil can already achieve high CE initially (98.09% between cycles 11 and 100). However, the CE for Cu foil starts to significantly degrade after 300 cycles, possibly due to the extensive SEI shell accumulation. When replacing the Cu foil with rGO framework, the first 100 cycles CE is far from satisfying (only 97.98%). This can be attributed to the Li deposition on its surface discussed above. With the usage of SirGO (stripping until 1.5 V *vs* Li/Li$^+$), not only the initial CE is promoted (99.09% between cycles 11 and 100) due to the nucleating effect, but long-term performance is also improved (100.25% between cycles 101 and 600). Nevertheless, another issue emerges, which is the increased CE fluctuation. Table 2 shows that the standard deviations of CE in both stages are amplified for SirGO. This is possibly caused by two factors. First, some Li$_x$Si particles are not in perfect electronic contact with the framework. Consequently, a small amount of Li might remain inactive within the Li$_x$Si alloy during a cycle but becomes active again during the next. Second, by stripping the Li-SirGO

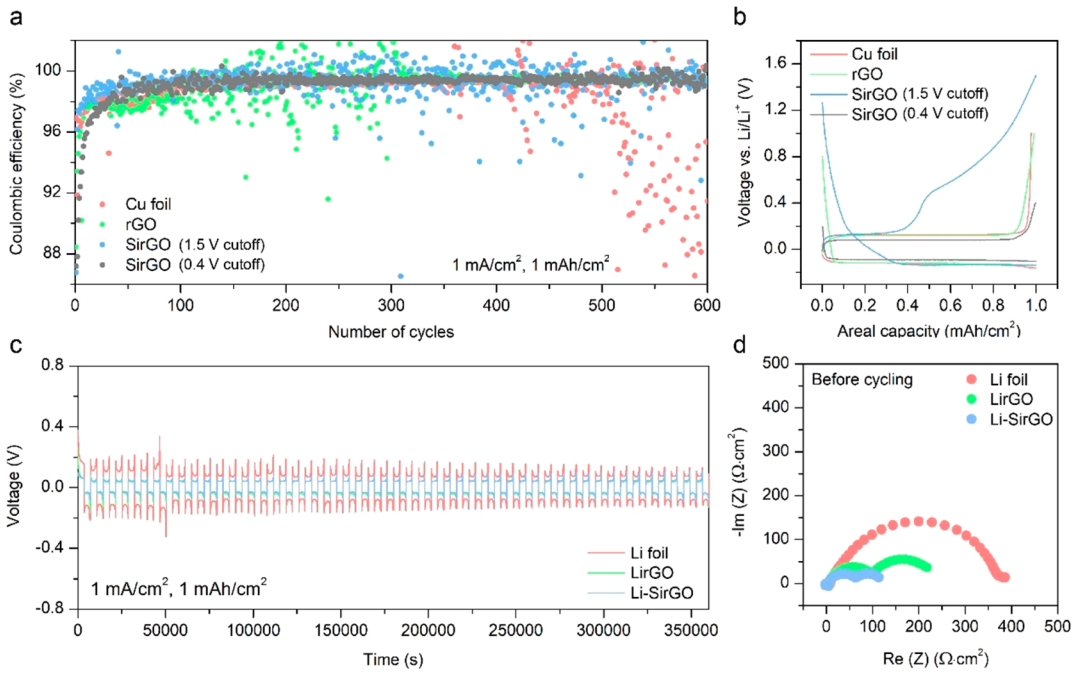

Figure 4. CE measurement and symmetric cell cycling results. (a) CE comparison between Cu foil, rGO film, and SirGO film (0.4 and 1.5 V as cutoff voltages). One M LiFSI/DME-TFEO is used as the electrolyte. (b) Voltage curves of the Li deposition and stripping of the samples in (a). (c) Voltage curves of the symmetric cell cycling with Li foil, Li-rGO or Li-SirGO as electrodes. One M LiPF$_6$/EC-DEC-FEC-VC is used as the electrolyte. (d) Impedance measurement results for the symmetric cells shown in (c) before cycling.

https://dx.doi.org/10.1021/acsnano.0c00184
ACS Nano 2020, 14, 4601−4608

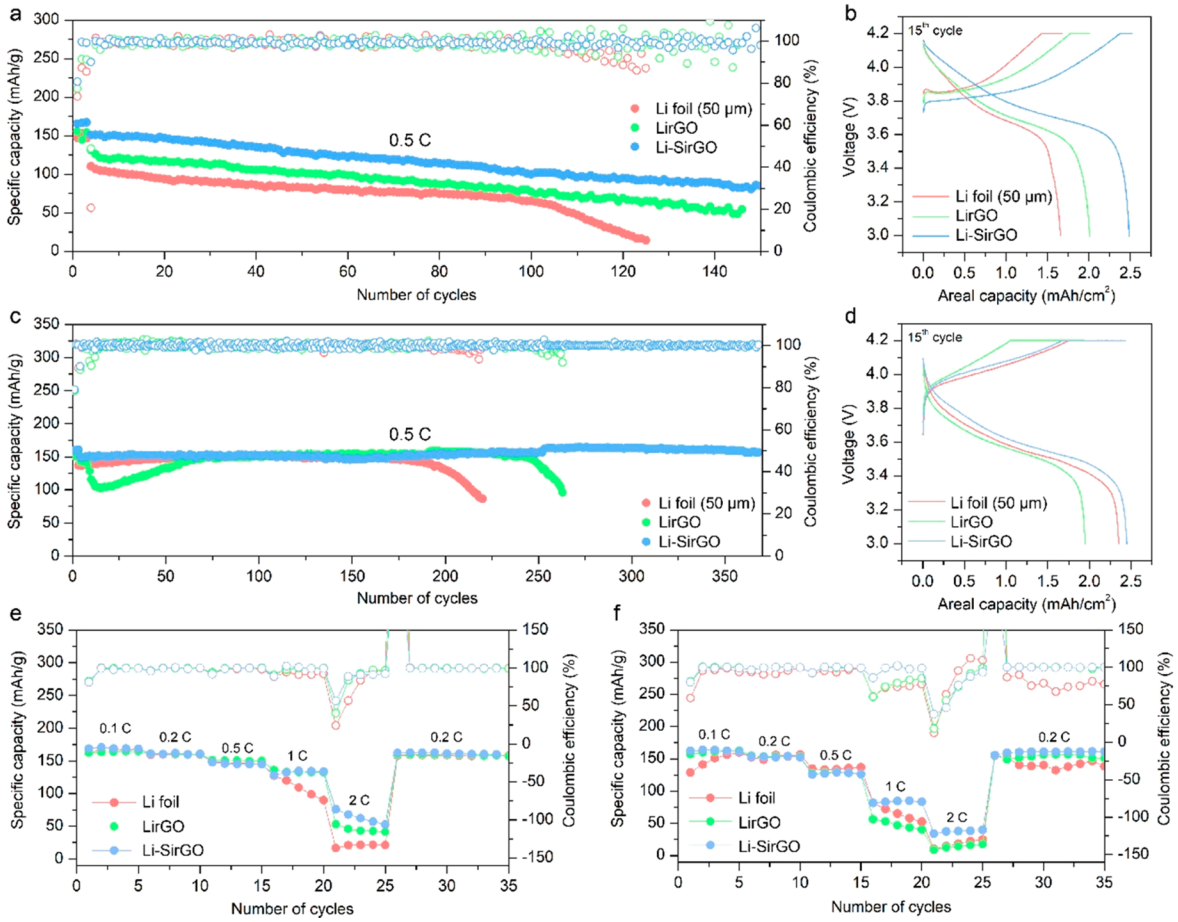

Figure 5. Full cell cycling results. (a, b) Long-term cycling performance and the charging/discharging curves (15th cycle) of full cells with NMC532 cathodes and Li foil, Li-rGO or Li-SirGO anodes. One M $LiPF_6$/EC-DEC-FEC-VC is used as the electrolyte. (c, d) Long-term cycling performance and the charging/discharging curves (15th cycle) of full cells with NMC532 cathodes and Li foil, Li-rGO or Li-SirGO anodes. One M LiFSI/DME-TFEO is used as the electrolyte. (e) Rate capability of full cells with NMC532 cathodes and Li foil, Li-rGO, or Li-SirGO anodes in 1 M $LiPF_6$/EC-DEC-FEC-VC electrolyte. (f) Rate capability of full cells with NMC532 cathodes and Li foil, Li-rGO, or Li-SirGO anodes in 1 M LiFSI/DME-TFEO electrolyte.

composite anode to 1.5 V *vs* Li/Li^+, we are extracting not only the metallic Li but also the Li within the alloy particles. In this way, the electrode thickness will not be well-maintained because the Si nanoparticles are too small to support the gaps between the graphene layers, leading to a pronounced variation of CE among cycles and the occasional over 100% CE. To fully take advantage of the merits of SirGO, another cycling method is designed. After formation cycles, the SirGO electrode is stepped to 0 V *vs* Li/Li^+ for a long time so that all Si particles are fully lithiated, while no metallic Li plates yet. The cycling starts afterward. In each cycle, 1 mAh/cm^2 of metallic Li is further deposited, and then the composite anode is stripped to only 0.4 V *vs* Li/Li^+. Under this condition, the voltage curves in Figure 4b confirm that only the metallic form of Li is cycled. In this way, improved CE of 99.40% is achieved with a very small fluctuation (0.247% standard deviation). Figure S7 shows that the long-term CE performance is also much improved under an increased areal capacity of 3 mAh/cm^2. These results confirm the crucial role of Si nanoparticles in the improved electrochemical performances.

Symmetric cell cycling is also performed with Li foil, Li-rGO, or Li-SirGO as Li electrodes. Using both 1 M $LiPF_6$/EC-DEC-FEC-VC (Figure 4c) and 1 M LiFSI/DME-TFEO electrolytes (Figure S8), the cell with Li-SirGO composite electrodes shows the least polarization. This is because the Li_xSi alloy particles enlarge some of the gaps and pore spaces within the composite anode framework, leading to a reduced local current density compared to bare Li foil. Besides, the overpotential of Li foil cell gradually decreases after long-term cycling, while that of the Li-SirGO cell remains low and stable. This indicates that the surface area of Li foil keeps increasing through dendritic growth and that of Li-SirGO remains rather stable. These observations agree well with the impedance measurement results. Before cycling, the impedance of the Li foil cell is much larger than that of the Li-SirGO cell with both electrolytes (Figures 4d and S5). After 100 cycles, however, the impedance of Li foil electrodes decreases by over 10 times (Figures S6 and S7). In contrast, the impedance of Li-SirGO decreases much more moderately. With 1 M LiFSI/DME-TFEO electrolyte, the impedance of the Li foil cell becomes even lower than that of the Li-SirGO cell (Figure S11b). This suggests that even though the Li deposition morphology appears to be very uniform in this electrolyte, high surface area still tends to build up vigorously without the usage of a "host" framework. These data imply that the Li-SirGO composite anode provides a reduced polarization during cycling without undermining the cycling efficiency, which is made possible

https://dx.doi.org/10.1021/acsnano.0c00184
ACS Nano 2020, 14, 4601−4608

through the suppressed dendritic growth and surface area build-up.

The improvement in electrochemical performance is further characterized in full cell measurements. Li foil, Li-rGO, and Li-SirGO (~10 mAh/cm^2) are paired with NMC532 cathodes (~2.5 mAh/cm^2) with 60 μL of electrolyte in a coin cell configuration. Long-term cycling is performed under 0.5C (1C = 2.5 mA/cm^2) after 3 formation cycles under 0.1C. In 1 M $LiPF_6$/EC-DEC-FEC-VC electrolyte, the specific capacity decays for all three types of anodes (Figure 5a). We speculate this is caused by the dendrite growth and resistance build-up on the Li anodes within this electrolyte. Nevertheless, the full cell with Li-SirGO composite anode provides both a higher and more stable capacity (~150 cycles of stable cycling compared to ~100 cycles of the cell with Li foil anode). On one hand, improved specific capacity is achieved through the increased surface area of the composite anode. This is further confirmed by the voltage curve during 15th cycle (Figure 5b), where the charging/discharging overpotential of the Li-SirGO cell is much smaller than the other cells. On the other hand, long-term cycling stability is realized by the improved CE of the Li-SirGO anode. With the usage of 1 M LiFSI/DME-TFEO electrolyte, the cycling performance is much improved (Figure 5c) due to its better protection for both the anode and cathode materials. Nevertheless, the Li-SirGO composite anode still provides the best performance, improving the full cell cycle life from ~200 cycles (Li foil anode) to ~380 cycles with negligible capacity decay. A repeatedly happening phenomenon for Li-rGO cells is that its capacity drops significantly and gradually restores at the initial stage of cycling (Figure 5c and Figure S12). Voltage curves of a Li-rGO cell in 15th cycle also show a much higher overpotential. We attribute this phenomenon to a non-ideal wettability of the 1 M LiFSI/DME-TFEO electrolyte to the Li-rGO composite anode. As a result, longer time is needed for the electrolyte to infiltrate into the pore spaces of the anode framework, leading to the gradual recovery of the capacity. This also explains previous data, where the symmetric cell with Li-rGO electrodes shows the highest impedance and overpotential after cycling within this electrolyte (Figures S4 and S7). Finally, the Li-SirGO cell shows the best rate capability in both electrolytes (Figure 5e,f), attributed to its high yet stable surface area. These results confirm the synergetic effect of a simultaneously engineered electrolyte and electrode architecture on the cycling performances. Not only the rechargeability can be further enhanced, but these composite anodes can also cycle at a reduced overpotential. This composite anode design will be especially beneficial for some recently developed electrolytes with excellent compatibility with metallic Li but reduced ionic conductivity.

CONCLUSION

The rGO "host" framework is further optimized by embedding Si nanoparticles between the graphene layers. This improves the composite anode through two crucial effects. First, Si serves as nucleation seeds for metallic Li so that Li can be guaranteed to deposit within the framework even without prestored Li. Second, by maintaining the composite anode potential lower than 0.4 V *vs* Li/Li$^+$, Li_xSi particles remain within the framework. They support the gaps between the graphene layers and enable a negligible thickness fluctuation. In addition to the electrode architecture design, we also pair the composite anode with a Li compatible electrolyte, achieving a stable cycling of a Li||NMC532 full cell for ~380 cycles with limited Li source. By combining electrolyte engineering with three-dimensional composite anodes, both higher cycling efficiency and better rate capability are achieved. This work demonstrates the importance of multicomponent engineering for the Li anode performance, achieves a significant advancement in Li anode cycling capability, and will inspire future studies for the realization of a commercial level high specific energy Li metal battery.

METHODS

Fabrication of Li-SirGO. Si nanoparticles (American Elements) were first dispersed into GO solutions (5 mg/mL, Graphene Supermarket) with a 1:4 mass ratio between Si and GO. The suspension was stirred overnight and sonicated for 30 min. Afterward, vacuum filtration was performed with nylon membranes (Whatman, with diameter of ~47 mm and pore size of ~0.2 μm). The as-obtained SiGO films were dried in a vacuum oven at 60 °C for 48 h and then transferred to an Ar-filled glovebox with subppm of O_2 level. To perform the spark reaction, Li foil (99.9%, Alfa Aesar) was first melted in a stainless-steel pan on a hot plate at ~400 °C. The SiGO films were then put into contact with the molten Li and the spark reaction occurred within seconds, forming SirGO films. The edges of the SirGO films were then brought into contact with the molten Li, which then infused into the SirGO films to form Li-SirGO composite films. These Li-SirGO films can act as electrodes once cooled down to room temperature.

Characterizations. SEM images were taken with an FEI Magellan 400 XHR. XRD characterizations were conducted on a Bruker D8 Venture with Cu radiation. The mass percentage of Si in SirGO films was determined from the weight loss curves measured under simulated air atmosphere (20% O_2 + 80% Ar) on a TG/DTA Instruments (Netzsch STA 449) with a heating rate of 5 °C/min. Under these conditions, mass increased due to slight Si oxidation, whereas carbon oxidation to gaseous species caused mass loss. To decouple these two processes, a pure Si control sample was measured at the same heating conditions, and the mass gain was deducted from the result of a SirGO sample during calculations.

Electrochemistry. All electrochemical characterizations in this work were performed with 2032-type coin cells (MTI) with 1 cm^2 electrodes and 60 μL of electrolyte. For half-cell CE measurements, Cu foil, rGO, or SirGO was used to pair with freshly scraped Li foil (99.9%, Alfa Aesar) electrodes. For symmetric cell cycling and impedance measurements, Li foil, Li-rGO, or Li-SirGO disks were used as both electrodes. For Li||NMC532 full cells, 50 μm Li foil, Li-rGO, or Li-SirGO (~10 mAh/cm^2) was paired with NMC532 cathodes (MTI, ~2.5 mAh/cm^2). The Li capacity in the composite anodes was controlled by optimizing the thickness of the vacuum filtered rGO or SirGO films. The electrolyte employed was either 1 M $LiPF_6$/EC-DEC-FEC-VC or 1 M LiFSI/DME-TFEO. The 1 M $LiPF_6$/EC-DEC-FEC-VC electrolyte was made by mixing 1 M $LiPF_6$/EC-DEC (Gotion) with FEC (Sigma-Aldrich) and VC (Sigma-Aldrich) by a mass ratio of 89:10:1. The 1 M LiFSI/DME-TFEO electrolyte was made by mixing LiFSI (Nippon), DME (Gotion), and TFEO (SynQuest). Celgard 2325 (25 μm PP/PE/PP) was used as the separator. Galvanostatic cycling was conducted on a LAND 8-channel battery tester. The impedance spectroscopy measurements were carried out on a Biologic VMP3 system. For the cycling of full cells, a constant current−constant voltage (CC−CV) procedure was used. For the long-term cycling, the CV process was set to finish when the current decays to 0.1C. For the rate capability measurement, the time for the CV process was set to be 20 min under all various rates.

ASSOCIATED CONTENT

Supporting Information

The Supporting Information is available free of charge at https://pubs.acs.org/doi/10.1021/acsnano.0c00184.

https://dx.doi.org/10.1021/acsnano.0c00184
ACS Nano 2020, 14, 4601−4608

SEM image of pristine Si nanoparticles, SEM-EDS mapping of Si distribution within the graphene layers, SEM images of the top-views of composite films, specific capacity measurements result, thickness measurement results of Li-SirGO film before and after metallic Li stripping, CE results at increased areal capacity, symmetric cell impedance measurements after cycling, and repeatability test for LirGO||NMC532 cells are provided (PDF)

AUTHOR INFORMATION

Corresponding Author

Yi Cui − *Department of Materials Science and Engineering, Stanford University, Stanford, California 94305, United States; Stanford Institute for Materials and Energy Sciences, SLAC National Accelerator Laboratory, Menlo Park, California 94305, United States;* orcid.org/0000-0002-6103-6352; Email: yicui@stanford.edu

Authors

Hansen Wang − *Department of Materials Science and Engineering, Stanford University, Stanford, California 94305, United States;* orcid.org/0000-0002-6738-1659

Xia Cao − *Energy and Environment Directorate, Pacific Northwest National Laboratory, Richland, Washington 99354, United States*

Hanke Gu − *Department of Materials Science and Engineering, Stanford University, Stanford, California 94305, United States*

Yayuan Liu − *Department of Materials Science and Engineering, Stanford University, Stanford, California 94305, United States;* orcid.org/0000-0002-0718-4784

Yanbin Li − *Department of Materials Science and Engineering, Stanford University, Stanford, California 94305, United States;* orcid.org/0000-0002-5285-8602

Zewen Zhang − *Department of Materials Science and Engineering, Stanford University, Stanford, California 94305, United States;* orcid.org/0000-0002-4909-4330

William Huang − *Department of Materials Science and Engineering, Stanford University, Stanford, California 94305, United States;* orcid.org/0000-0001-8717-5337

Hongxia Wang − *Department of Materials Science and Engineering, Stanford University, Stanford, California 94305, United States;* orcid.org/0000-0003-0720-3305

Jiangyan Wang − *Department of Materials Science and Engineering, Stanford University, Stanford, California 94305, United States;* orcid.org/0000-0001-6951-1296

Wu Xu − *Energy and Environment Directorate, Pacific Northwest National Laboratory, Richland, Washington 99354, United States;* orcid.org/0000-0002-2685-8684

Ji-Guang Zhang − *Energy and Environment Directorate, Pacific Northwest National Laboratory, Richland, Washington 99354, United States;* orcid.org/0000-0001-7343-4609

Complete contact information is available at: https://pubs.acs.org/10.1021/acsnano.0c00184

Author Contributions

Ha.W. and Y.C. conceived the idea and designed the experiments, with suggestion from W.X. and J.-G.Z. Ha.W. performed electrochemical measurements. X.C. prepared the Li compatible electrolyte. Ha.W., H.G., and Y.L. conducted material fabrications. Z.Z. and W.H. performed SEM and EDS characterizations of the samples. Ho.W. conducted XRD characterizations. J.W. performed thermogravimetric analysis. All authors contributed to the manuscript writing.

Notes

The authors declare no competing financial interest.

ACKNOWLEDGMENTS

The work on layered host materials was funded by the Materials Sciences and Engineering Division of the Basic Energy Sciences office at the US Department of Energy, under contract DEAC02-76- SFO0515. This host material research was initiated by the support from the Assistant Secretary for Energy Efficiency and Renewable Energy, Office of Vehicle Technologies of the U.S. Department of Energy under the Battery Materials Research (BMR) program and Battery 500 Consortium. The electrolyte part of the work is supported by the Assistant Secretary for Energy Efficiency and Renewable Energy, Office of Vehicle Technologies of the U.S. Department of Energy under the Battery 500 Consortium. We thank Karim Zaghib and Hydro-Québec for providing the thin Li foil used in the full cell testing.

REFERENCES

(1) Lin, D.; Liu, Y.; Cui, Y. Reviving the Lithium Metal Anode for High-Energy Batteries. *Nat. Nanotechnol.* **2017**, *12*, 194−206.

(2) Liu, Y.; Zhou, G.; Liu, K.; Cui, Y. Design of Complex Nanomaterials for Energy Storage: Past Success and Future Opportunity. *Acc. Chem. Res.* **2017**, *50*, 2895−2905.

(3) Liu, B.; Zhang, J.-G.; Xu, W. Advancing Lithium Metal Batteries. *Joule* **2018**, *2*, 833−845.

(4) Cheng, X.-B.; Zhang, R.; Zhao, C.-Z.; Zhang, Q. Toward Safe Lithium Metal Anode in Rechargeable Batteries: A Review. *Chem. Rev.* **2017**, *117*, 10403−10473.

(5) Xu, W.; Wang, J.; Ding, F.; Chen, X.; Nasybulin, E.; Zhang, Y.; Zhang, J.-G. Lithium Metal Anodes for Rechargeable Batteries. *Energy Environ. Sci.* **2014**, *7*, 513−537.

(6) Wang, H.; Liu, Y.; Li, Y.; Cui, Y. Lithium Metal Anode Materials Design: Interphase and Host. *Electrochem. Energy Rev.* **2019**, *2*, 509−517.

(7) Yan, K.; Lu, Z.; Lee, H.-W.; Xiong, F.; Hsu, P.-C.; Li, Y.; Zhao, J.; Chu, S.; Cui, Y. Selective Deposition and Stable Encapsulation of Lithium Through Heterogeneous Seeded Growth. *Nat. Energy* **2016**, *1*, 16010.

(8) Lin, D.; Liu, Y.; Liang, Z.; Lee, H.-W.; Sun, J.; Wang, H.; Yan, K.; Xie, J.; Cui, Y. Layered Reduced Graphene Oxide With Nanoscale Interlayer Gaps as a Stable Host for Lithium Metal Anodes. *Nat. Nanotechnol.* **2016**, *11*, 626−632.

(9) Wang, H.; Lin, D.; Xie, J.; Liu, Y.; Chen, H.; Li, Y.; Xu, J.; Zhou, G.; Zhang, Z.; Pei, A.; Zhu, Y.; Liu, K.; Wang, K.; Cui, Y. An Interconnected Channel-Like Framework as Host for Lithium Metal Composite Anodes. *Adv. Energy Mater.* **2019**, *9*, 1802720.

(10) Wang, H.; Lin, D.; Liu, Y.; Li, Y.; Cui, Y. Ultrahigh-Current Density Anodes with Interconnected Li Metal Reservoir Through Overlithiation of Mesoporous AlF_3 Framework. *Sci. Adv.* **2017**, *3*, No. e1701301.

(11) Wang, H.; Li, Y.; Li, Y.; Liu, Y.; Lin, D.; Zhu, C.; Chen, G.; Yang, A.; Yan, K.; Chen, H.; Zhu, Y.; Li, J.; Xie, J.; Xu, J.; Zhang, Z.; Vilá, R.; Pei, A.; Wang, K.; Cui, Y. Wrinkled Graphene Cages as Hosts for High-Capacity Li Metal Anodes Shown by Cryogenic Electron Microscopy. *Nano Lett.* **2019**, *19*, 1326−1335.

(12) Zhang, R.; Chen, X.; Shen, X.; Zhang, X.-Q.; Chen, X.-R.; Cheng, X.-B.; Yan, C.; Zhao, C.-Z.; Zhang, Q. Coralloid Carbon Fiber-Based Composite Lithium Anode for Robust Lithium Metal Batteries. *Joule* **2018**, *2*, 764−777.

(13) Li, G.; Liu, Z.; Huang, Q.; Gao, Y.; Regula, M.; Wang, D.; Chen, L.-Q.; Wang, D. Stable Metal Battery Anodes Enabled by

Polyethylenimine Sponge Hosts by Way of Electrokinetic Effects. *Nat. Energy* **2018**, *3*, 1076−1083.
(14) Liu, Y.; Lin, D.; Liang, Z.; Zhao, J.; Yan, K.; Cui, Y. Lithium-Coated Polymeric Matrix as a Minimum Volume-Change and Dendrite-Free Lithium Metal Anode. *Nat. Commun.* **2016**, *7*, 10992.
(15) Lin, D.; Zhao, J.; Sun, J.; Yao, H.; Liu, Y.; Yan, K.; Cui, Y. Three-Dimensional Stable Lithium Metal Anode with Nanoscale Lithium Islands Embedded in Ionically Conductive Solid Matrix. *Proc. Natl. Acad. Sci. U. S. A.* **2017**, *114*, 4613−4618.
(16) Liang, Z.; Lin, D.; Zhao, J.; Lu, Z.; Liu, Y.; Liu, C.; Lu, Y.; Wang, H.; Yan, K.; Tao, X.; Cui, Y. Composite Lithium Metal Anode by Melt Infusion of Lithium into a 3D Conducting Scaffold with Lithiophilic Coating. *Proc. Natl. Acad. Sci. U. S. A.* **2016**, *113*, 2862−2867.
(17) Niu, C.; Pan, H.; Xu, W.; Xiao, J.; Zhang, J.-G.; Luo, L.; Wang, C.; Mei, D.; Meng, J.; Wang, X.; Liu, Z.; Mai, L.; Liu, J. Self-Smoothing Anode for Achieving High-Energy Lithium Metal Batteries under Realistic Conditions. *Nat. Nanotechnol.* **2019**, *14*, 594−601.
(18) Xu, K. Electrolytes and Interphases in Li-Ion Batteries and Beyond. *Chem. Rev.* **2014**, *114*, 11503−11618.
(19) Jiao, S.; Ren, X.; Cao, R.; Engelhard, M. H.; Liu, Y.; Hu, D.; Mei, D.; Zheng, J.; Zhao, W.; Li, Q.; Liu, N.; Adams, B. D.; Ma, C.; Liu, J.; Zhang, J.-G.; Xu, W. Stable Cycling of High-Voltage Lithium Metal Batteries in Ether Electrolytes. *Nat. Energy* **2018**, *3*, 739−746.
(20) Ren, X.; Zou, L.; Jiao, S.; Mei, D.; Engelhard, M. H.; Li, Q.; Lee, H.; Niu, C.; Adams, B. D.; Wang, C.; Liu, J.; Zhang, J.-G.; Xu, W. High-Concentration Ether Electrolytes for Stable High-Voltage Lithium Metal Batteries. *ACS Energy Lett.* **2019**, *4*, 896−902.
(21) Qian, J.; Henderson, W. A.; Xu, W.; Bhattacharya, P.; Engelhard, M.; Borodin, O.; Zhang, J.-G. High Rate and Stable Cycling of Lithium Metal Anode. *Nat. Commun.* **2015**, *6*, 6362.
(22) Fan, X.; Chen, L.; Borodin, O.; Ji, X.; Chen, J.; Hou, S.; Deng, T.; Zheng, J.; Yang, C.; Liou, S.-C.; Amine, K.; Xu, K.; Wang, C. Non-Flammable Electrolyte Enables Li-Metal Batteries with Aggressive Cathode Chemistries. *Nat. Nanotechnol.* **2018**, *13*, 715−722.
(23) Ren, X.; Zou, L.; Cao, X.; Engelhard, M. H.; Liu, W.; Burton, S. D.; Lee, H.; Niu, C.; Matthews, B. E.; Zhu, Z.; Wang, C.; Arey, B. W.; Xiao, J.; Liu, J.; Zhang, J.-G.; Xu, W. Enabling High-Voltage Lithium-Metal Batteries under Practical Conditions. *Joule* **2019**, *3*, 1662−1676.
(24) Yu, L.; Chen, S.; Lee, H.; Zhang, L.; Engelhard, M. H.; Li, Q.; Jiao, S.; Liu, J.; Xu, W.; Zhang, J.-G. A Localized High-Concentration Electrolyte with Optimized Solvents and Lithium Difluoro(oxalate)-borate Additive for Stable Lithium Metal Batteries. *ACS Energy Lett.* **2018**, *3*, 2059−2067.
(25) Chen, S.; Zheng, J.; Yu, L.; Ren, X.; Engelhard, M. H.; Niu, C.; Lee, H.; Xu, W.; Xiao, J.; Liu, J.; Zhang, J.-G. High-Efficiency Lithium Metal Batteries with Fire-Retardant Electrolytes. *Joule* **2018**, *2*, 1548−1558.
(26) Chen, S.; Zheng, J.; Mei, D.; Han, K. S.; Engelhard, M. H.; Zhao, W.; Xu, W.; Liu, J.; Zhang, J.-G. High-Voltage Lithium-Metal Batteries Enabled by Localized High-Concentration Electrolytes. *Adv. Mater.* **2018**, *30*, 1706102.
(27) Ren, X.; Chen, S.; Lee, H.; Mei, D.; Engelhard, M. H.; Burton, S. D.; Zhao, W.; Zheng, J.; Li, Q.; Ding, M. S.; Schroeder, M.; Alvarado, J.; Xu, K.; Meng, Y. S.; Liu, J.; Zhang, J.-G.; Xu, W. Localized High-Concentration Sulfone Electrolytes for High-Efficiency Lithium-Metal Batteries. *Chem.* **2018**, *4*, 1877−1892.
(28) Cao, X.; Ren, X.; Zou, L.; Engelhard, M. H.; Huang, W.; Wang, H.; Matthews, B. E.; Lee, H.; Niu, C.; Arey, B. W.; Cui, Y.; Wang, C.; Xiao, J.; Liu, J.; Xu, W.; Zhang, J.-G. Monolithic Solid-Electrolyte Interphases Formed in Fluorinated Orthoformate-Based Electrolytes Minimize Li Depletion and Pulverization. *Nat. Energy* **2019**, *4*, 796−805.
(29) Lipatov, A.; Guinel, M. J.-F.; Muratov, D. S.; Vanyushin, V. O.; Wilson, P. M.; Kolmakov, A.; Sinitskii, A. Low-temperature Thermal Reduction of Graphene Oxide: *In Situ* Correlative Structural, Thermal Desorption, and Electrical Transport Measurement. *Appl. Phys. Lett.* **2018**, *112*, 053103.

https://dx.doi.org/10.1021/acsnano.0c00184
ACS Nano 2020, 14, 4601−4608